Clim Dyn
DOI 10.1007/s00382-013-1954-y

Interpreting observed northern hemisphere snow trends with large ensembles of climate simulations

L. R. Mudryk · P. J. Kushner · C. Derksen

Received: 5 March 2013 / Accepted: 23 September 2013

Abstract Simulated variability and trends in Northern Hemisphere seasonal snow cover are analyzed in large ensembles of climate integrations of the National Center for Atmospheric Research's Community Earth System Model. Two 40-member ensembles driven by historical radiative forcings are generated, one coupled to a dynamical ocean and the other driven by observed sea surface temperatures (SSTs) over the period 1981–2010. The simulations reproduce many aspects of the observed climatology and variability of snow cover extent as characterized by the NOAA snow chart climate data record. Major features of the simulated snow water equivalent (SWE) also agree with observations (GlobSnow Northern Hemisphere SWE data record), although with a lesser degree of fidelity. Ensemble spread in the climate response quantifies the impact of natural climate variability in the presence and absence of coupling to the ocean. Both coupled and uncoupled ensembles indicate an overall decrease in springtime snow cover that is consistent with observations, although springtime trends in most climate realizations are weaker than observed. In the coupled ensemble, a tendency towards excessive warming in wintertime leads to a strong wintertime snow cover loss that is not found in observations. The wintertime warming bias and snow cover reduction trends are reduced in the uncoupled ensemble with observed SSTs. Natural climate variability generates widely different regional patterns of snow trends across realizations; these patterns are related in an intuitive way to temperature, precipitation and circulation trends in individual realizations. In particular, regional snow loss over North America in individual realizations is strongly influenced by North Pacific SST trends (manifested as Pacific Decadal Oscillation variability) and by sea level pressure trends in the North Pacific/North Atlantic sectors.

Keywords Climate change · Snow · Climate models · Pacific decadal oscillation

L. R. Mudryk (✉) · P. J. Kushner
Department of Physics, University of Toronto, 60 St. George Street, Toronto, ON M5S 1A7, Canada
e-mail: mudryk@atmosp.physics.utoronto.ca

C. Derksen
Climate Research Division, Environment Canada, 4905 Dufferin Street, Toronto, ON M3H 5T4, Canada

1 Introduction

Seasonal snow cover is a key element of the Northern Hemisphere's energy and water balance and contributes via albedo feedbacks to global climate sensitivity. In response to greenhouse gas forcing, Northern Hemisphere snow cover extent (SCE) is projected to decrease (Groisman et al. 1994) while snowfall is projected to decrease at midlatitudes (due to precipitation phase relationships with increasing temperatures) but increase at high latitudes (due to projected changes in atmospheric water vapour, Räisänen 2008). Reliable decadal to multidecadal prediction of seasonal snow cover on regional and larger scales is predicated on the ability to properly simulate historical changes and separate forced signals from natural climate variability. In this context, we examine two large-ensemble hindcasts of a global climate model (GCM), the National Center for Atmospheric Research's Community Earth System Model (CCSM4), in comparison with observations. Each ensemble member represents an independent climate realization that can be compared to the observed climate record (which represents, in a statistical sense, only one of many possible climate realizations). The design of this

Published online: 18 October 2013

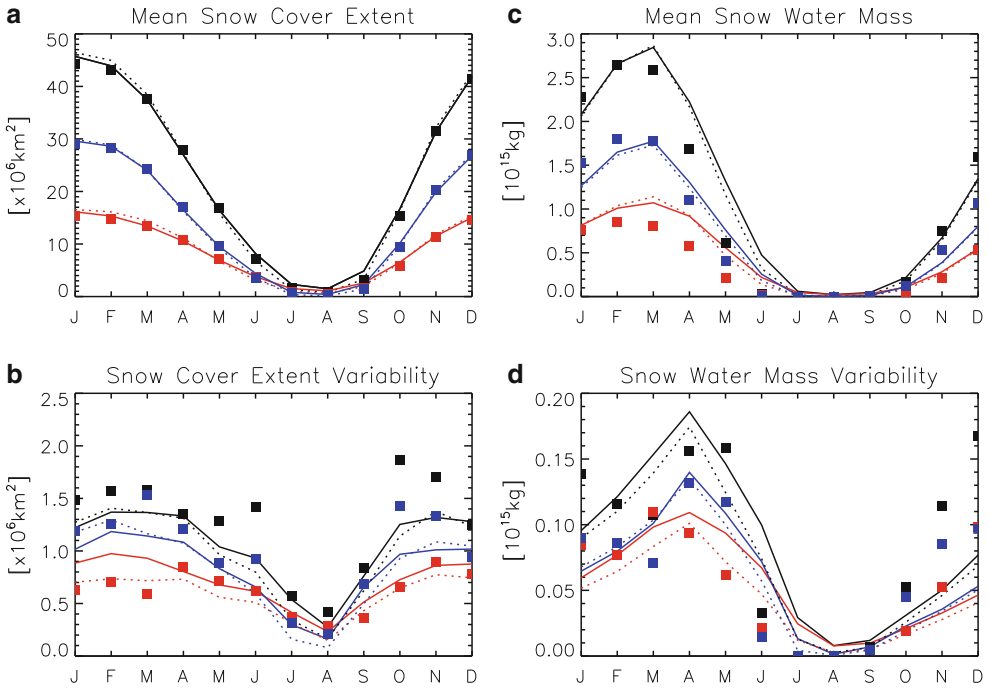

Fig. 1 **a** Annual cycle of snow cover extent (SCE) for NH (*black*), NA (*red*), and EUR (*blue*) regions for NOAA snow chart CDR (*squares*), ensemble mean `coupled` experiment (*solid*), and ensemble mean `uncoupled` experiment (*dotted*). **b** As (**a**) for observed interannual variability and ensemble mean of interannual variability of individual realizations of the simulations. **c**–**d** As (**a**)–(**b**) for GlobSnow and simulated SWE. Individual time series are detrended prior to calculating interannual variability

experiment is similar to work by Deser et al. (2012), who quantified the role of natural climate variability in future projections of temperature trends.

Observed trends of snow-related quantities show large variability in sign and magnitude that depends on the snow cover variable, region of focus, season, and time period (see Fig. 1 in Brown and Mote 2009, for example). Seasonal snow cover duration is expected to be one of the variables most responsive to climate change (Brown and Mote 2009); and, while little change in the onset date of snow in boreal autumn has been observed (hereafter all seasonal references are with respect to boreal climate), there is a marked trend towards earlier springtime snow-off dates in the observations (Derksen and Brown 2012a). This trend is echoed in the trends of satellite derived springtime SCE (Déry and Brown 2007), which are occurring in parallel with NH land surface warming. For the period 1979–2011, Derksen and Brown (2012b) report decreasing NH June SCE of ~ -18 % decade^{-1}, driven by particularly strong SCE reductions over the past decade. Trends in snow water equivalent (SWE) are complicated by their dependence on temperature and precipitation trends. For example, Bulygina et al. (2010) report increased SWE over Eurasian and northern Russia over the period 1966–2009 while Atkinson et al. (2006) report decreased SWE over northern Canada during the period 1966–1996, despite both regions showing increased cold season precipitation (Callaghan et al. 2010; Trenberth et al. 2007; Min et al. 2008).

It is challenging to separate anthropogenically forced trends in seasonal snow cover from trends reflecting natural climate variability. For example, it is not clear if the recent dramatic SCE reduction trends reported by Derksen and Brown (2012b) reflect anthropogenic forcing or natural climate variability. Natural modes of climate variability, like the Pacific North American (PNA) and Pacific Decadal Oscillation (PDO) patterns, can influence North American snow cover—positive phases of the PNA and PDO are associated with reduced snow accumulation and a shorter snow cover season (Derksen et al. 2007; Gutzler and Rosen 1992; Brown and Goodison 1996). Furthermore, Eurasian snow accumulation correlates positively with cyclone frequency and negatively with anticyclones (blocks); trends in these phenomena explain portions of the variability and trends in Eurasian snow depth since the 1950s (Popova 2004, 2007). The challenge of determining forced circulation trends that influence snow cover compounds the challenge of determining the influence of the forced component of temperature and precipitation trends.

In this study we compare an ensemble of independent but identically forced realizations of model simulations to the single observed realization of climate. This allows us to assess what aspects of recent changes in seasonal snow

cover are captured in the simulations while accounting for climate variability. We analyze snow cover climatology, variability, and trends in two different configurations of CCSM4. The first configuration is the coupled version of CCSM4 in which the atmosphere is coupled to dynamical ocean and sea ice components. The second configuration prescribes observed sea surface temperatures (SST) and sea ice. The differences between these two versions allow us to isolate the influence of SST and sea ice trends on the resulting simulated trend patterns. While we expect the direct influence of such differing SST/sea ice trends to dominant the differences between the coupled and uncoupled simulations, we note that ocean-atmosphere coupling may also contribute. To the extent that the model resembles the real world, each individual realization represents a potential historical evolution of the climate, with individual realizations demonstrating the range of trends possible as a result of natural variability.

We organize the remainder of this paper as follows. In Sect. 2 we describe the experimental setup of the models, the observational data used, and analysis techniques. In Sect. 3 we compare results from both experimental setups against one another and observations. We conclude in Sect. 4.

2 Data and methods

2.1 Model configurations

We use Version 1.0.2 of the National Center for Atmospheric Research (NCAR) Community Earth System Model (CESM) in two configurations. The first configuration is the standard Community Climate System 4 (CCSM4) with the Community Atmosphere Model 4 (CAM4), the Community Land Model 4 (CLM4), the Community Ice Code 4 (CICE4) and the Parallel Ocean Program 2 (POP2) (see Gent et al. 2011 and http://www.cesm.ucar.edu/). The atmosphere and land model are run on a nominally two-degree finite volume grid provided with the tag f19 in the Version 1.0.2 code release; the ocean and ice models are run on the nominally 1 degree Greenland dipole grid (g16). The two-degree atmosphere/land grid resolution is coarser than the standard nominally 1 degree resolution of CCSM4 used in Gent et al. 2011 and Lawrence et al. 2012; it is chosen to reduce computational cost of carrying out the large ensemble with available resources. This configuration will be referred to as coupled, where it is understood that the atmosphere is coupled to a dynamical ocean and sea ice model. The second configuration uses the same atmosphere and land models, however global sea ice concentration and sea surface temperatures (SSTs) are prescribed using the Atmospheric Model Intercomparison Project (AMIP) observed SST and sea ice data provided by NCAR (Hurrell et al. 2008). This prescribed SST and sea ice configuration will be referred to as uncoupled.

For coupled and uncoupled configurations we perform forty historical climate realizations forced with identical time-dependent historical greenhouse gases, ozone, aerosols, volcanic emissions and solar variability. The data for these prescriptions are the standard data sets provided by NCAR and are consistent with the historical radiative forcing CMIP5 protocol (Taylor et al. 2012), apart from an adjustment we make to merge the forcing time series at 2005 with those of the 4.5W Representative Concentration Pathway (rcp45) in order to extend the runs from January 2006 to December 2010. In the case of the uncoupled experiment, at the time of running these simulations SST and sea ice forcing data were only available to December 2008, which limits our simulations to that point.

All realizations in the coupled experiment are derived from a January 1955 climate state taken from a 'parent-run' branched in 1850 from a pre-industrial control and then run forward from January 1850 using historical forcing. Starting January 1955, slightly distinct climate states are created by altering the least-significant bit of a single atmospheric variable at a single grid location. The effects of this perturbation propagate rapidly throughout the simulated climate. Based on results by Branstator and Teng (2010) we estimate that the realizations should be statistically independent within a decade (often much faster based on estimates of the Lyaponov timescale). Comparisons of long time scale climate system indices such as the Atlantic Mean Overturning Circulation, El Nino Southern Oscillation and Pacific Decadal Oscillation as well as global mean surface temperature time series confirm this assumption. We discard the first 26 years of the simulation and analyze output from 1981-2010 which ensures that the realizations are statistically independent apart from the common forcing and that the analysis period overlaps with relatively high quality snow observations from the satellite era (1967 onwards for SCE; 1979 onwards for SWE).

Independent realizations for the uncoupled experiment were created in a similar manner, except that the parent run was initialized starting in 1950 from an unequilibrated state. A five year lead time is sufficient for land and atmospheric processes to equilibrate since they have much shorter intrinsic time scales than the ocean and sea ice components of the climate system.

2.2 Observational and model data

The fractional grid area covered by snow (snow cover fraction or SCF) and SCE data are from the NOAA snow

chart climate data record (CDR, Brown and Robinson 2011), a time series derived primarily by optical satellite imagery and housed at the Rutgers University Global Snow Lab (http://climate.rutgers.edu/snowcover/). Brown and Derksen (2013) have shown that there is an October snow cover bias over a portion of the record that is not seen in other data sources. The bias leads to spurious trends in the Eurasian region if not accounted for. During October we supplement the NOAA CDR with bias-adjusted Eurasian data used in the above publication and in situ Russian data (Bulygina et al. 2009), both available over the period 1982–2010.

SWE data are from the European Space Agency GlobSnow project (version 1.3), derived through a combination of satellite passive microwave data, forward snow emission model simulations, and climate station observations for non-alpine regions of the northern hemisphere (Takala et al. 2011). Due to inconsistencies in North American climate station data in 1981, we limit the SWE data to 1982-2010.

Observed temperature records are from the University of East Anglia Climate Research Unit (UEA-CRU) version CRUTEM4 (Jones et al. 2012).

Model data available for each grid cell consists of SCF, SWE, surface air temperature/sea surface temperature, sea level pressure, and snow water precipitation defined in a manner consistent with the observational products but on the model grid.

2.3 Analysis methods

Time series analysis is carried out over three land masses: all Northern Hemisphere land mass north of 30N (referred to as NH), the North American continent north of 30N (NA), and the Eurasian continent north of 30N (EUR). We exclude the Greenland land mass from all three definitions. SCE time series are derived by summing the total land area under snow over NH, NA, and EUR. Land surface temperature time series are calculated as area weighted means over the three regions. Snow water mass (SWM) time series (or equivalently snow water volume) are derived by multiplying the grid box SWE by grid box area and summing the result over NH, NA, and EUR. We convert volume to mass units using the density of water. The SWM calculations neglect snow on land ice sheets in the Canadian Archipelago as well as the Russian Arctic islands. We also use the same elevation mask applied in the GlobSnow data processing chain to remove alpine regions, for which SWE retrievals are highly uncertain in the GlobSnow product.

We use these time series to calculate climatologies, anomalies, standard deviations and linear trends. We treat each ensemble member as a possible climate realization that can be compared to the observed climate. Accordingly, we calculate interannual variability and statistical significance of trends independently for individual realizations just as one does with the observational record. We then examine the mean and variability of the these statistics in the ensemble to assess whether observations and simulations are consistent.

Finally, we also present maps of trends in SCF and SWE in each grid cell, and of trends in model SLP and surface air temperature. These trends are either for individual realizations or are ensemble averaged, as described in the text. Stippling is superimposed on these maps to mark regions with trends significantly different from zero based on a two-sided t-test with a 95 % confidence level. In determining the test statistic, we use variance sampled from the detrended anomalies of the ensemble mean, particular realization, or selected subset of realizations, as appropriate for the trends being displayed.

3 Results

3.1 Observed and simulated seasonal snow cover

The simulated annual cycle of SCE in the coupled and uncoupled experiments is realistic for the Northern Hemisphere regions NH, NA, and EUR (Fig. 1a). Small biases with respect to observations and differences between the coupled and uncoupled experiments are consistent with biases in land surface temperature (not shown). Lawrence et al. (2011) find that SCE in CCSM4 is greatly improved compared to previous CCSM generations. We find that the SCE simulation is not greatly affected at the continental scale by using our two degree version of the model instead of the standard one degree version. The models' interannual variability in SCE (that is, the ensemble average of the interannual variability of detrended time series from individual realizations) is generally less than or similar to the observed (Fig. 1b) throughout the year. The coupled experiment's interannual variability in NA is somewhat larger than the uncoupled experiment's but this effect is not evident for the more continental climate of EUR. Both model ensembles underestimate SCE variability in the Subartic and Arctic during the transitional months of June (month of maximum observed seasonal SCE decline) and October (month of maximum seasonal SCE increase). This discrepancy is related to the inability of climate models to adequately capture the magnitude of variability during the high latitude snow melt and snow onset periods (Derksen and Brown 2012b).

The SWE climatology simulated in the coupled and uncoupled experiments is reasonable, however there is a positive bias in the spring season (AMJ) SWE over both

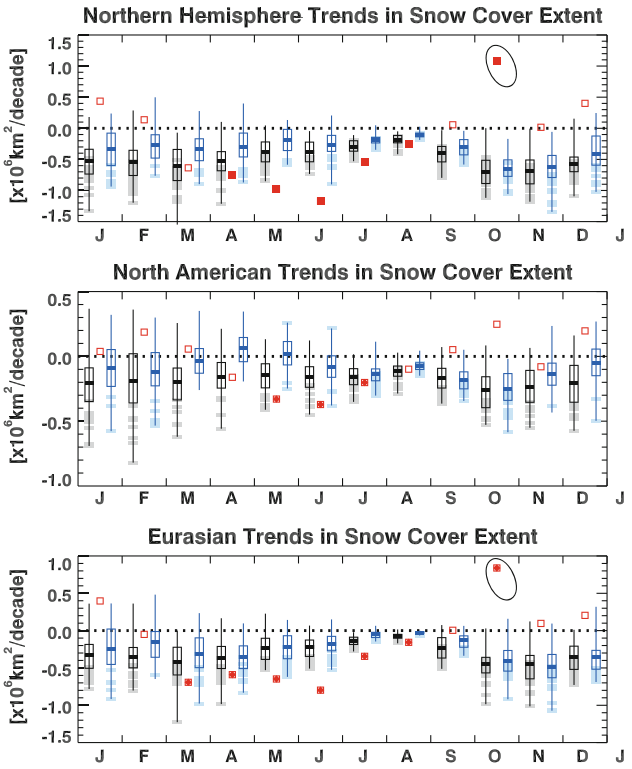

Fig. 2 Annual cycle of SCE trends for NOAA snow chart CDR (*red*), coupled (*black*) experiment, and uncoupled (*blue*) experiment, for NH (*top*), NA (*middle*), and EUR (*bottom*). For the simulations, the extent of the *vertical lines* represents the range of trends for the 40 ensemble members, *boxes* span the interquartile range (25th and 75th percentiles), and *dashes* mark the median trends. Individual realizations with a significant trend (based on 95 % confidence intervals using the interannual variability of that realization) are marked with a *shaded horizontal bar*. Signficant observed trends are indicated with a *solid* instead of an *open red square*. Encircled observational trends from October are prominently biased and discussed further in the text and Fig. 5

continents (Fig. 1c). In addition, the seasonal maximum in SWE is shifted towards March in the models for both continents instead of February in the GlobSnow data. A similar difference is apparent with respect to variability, where the observational peak in North American variability occurs in April in the models rather than March. The simulations underestimate interannual variability in SWE in October-November-December for EUR and NH.

Generally, the CCSM4 model appears to adequately capture the principal features of seasonal snow cover for our purposes, especially compared to previous generations of climate models (e.g. Frei and Robinson 1998; e.g. Frei et al. 2003). Observational uncertainty must also be accounted for when considering the assessment of the model simulations. In general, uncertainty associated with SCE is less than with SWE. The SCE datasets and the errors therein are now reasonably well understood because of the evaluation of multiple datasets (Brown et al. 2007,

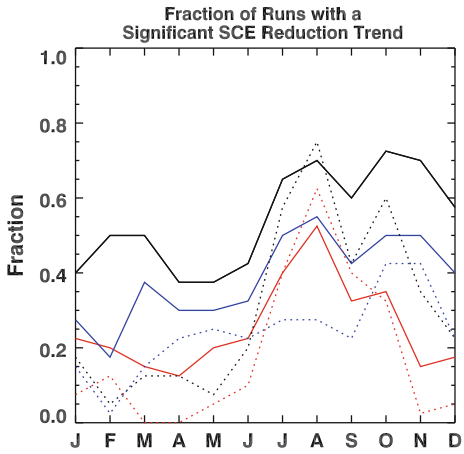

Fig. 3 Fraction of ensemble members with significant SCE reduction trends in NH (*black*), NA (*red*), and EUR (*blue*) SCE, for coupled (*solid*) experiment and uncoupled (*dotted*) experiment

2010; Brown and Robinson 2011). In fact, recently highlighted biases in the NOAA snow cover CDR (Brown and Derksen 2013) have been discovered because of the comparatively better understanding of the SCE data sets and comparisons among them. Uncertainty in SWE observations are comparatively less constrained because of both the difficulties associated with deriving this variable (unlike binary SCE products, SWE uncertainties can

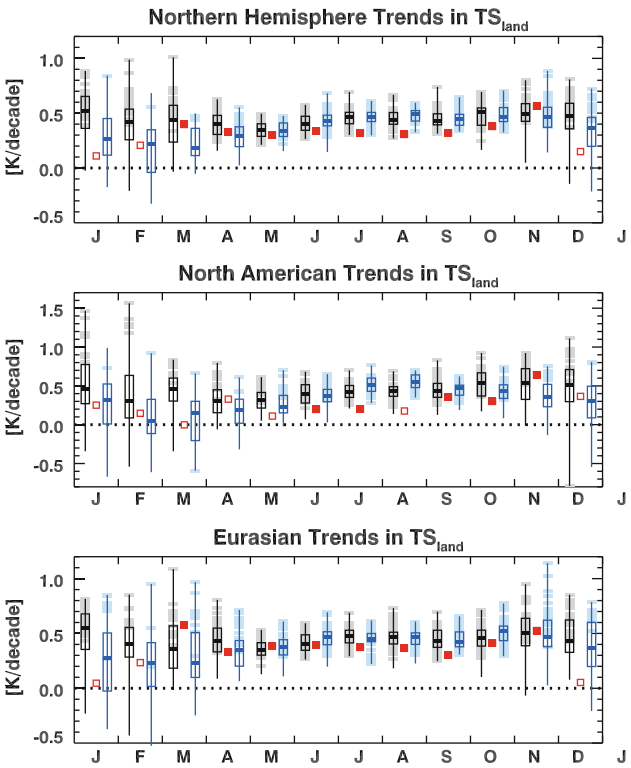

Fig. 4 As Fig. 2, but for simulated and CRU land surface temperature

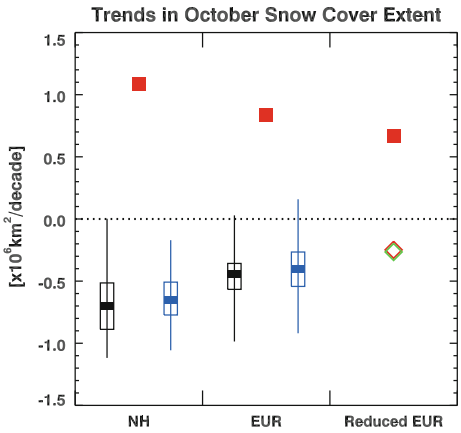

Fig. 5 October SCE trends for three differing geographical regions. Simulated trends from the `coupled` (*black*) and `uncoupled` (*blue*) experiments and trends from unadjusted NOAA CDR (*red squares*) as in Fig. 2 for NH and EUR regions. Also shown are trends over the reduced portion of Eurasia analyzed in the Brown and Derksen (2013) study based on: unadjusted NOAA time series (*red square*), adjusted NOAA time series (*red diamond*), and in situ observations (*green diamond*). Significant observed trends are indicated with *filled symbols*

accumulate through the snow season) and relatively fewer inter-dataset comparisons (Clifford, 2010).

3.2 Trends in snow cover extent and fraction

The annual cycle of SCE trends for NH, NA, and EUR are shown for the observations (squares) and simulations (box plots) in Fig. 2. In the box plots the full range and statistical significance of trends in individual realizations are shown for the coupled (grey) and uncoupled (blue) model experiments (see caption for details). For observed SCE, statistically significant reductions are seen in AMJJA for NH, MJJ for NA, and MAMJJA for EUR. These observational trends have been documented in previous studies (for instance, Brown and Robinson 2011; Derksen and Brown 2012b).

In the coupled ensemble (black box plots), the vast majority of the individual realizations have snow reduction trends throughout the entire year and across all three regions. (The blue box plots represent the uncoupled simulations and will be discussed below.) In particular,

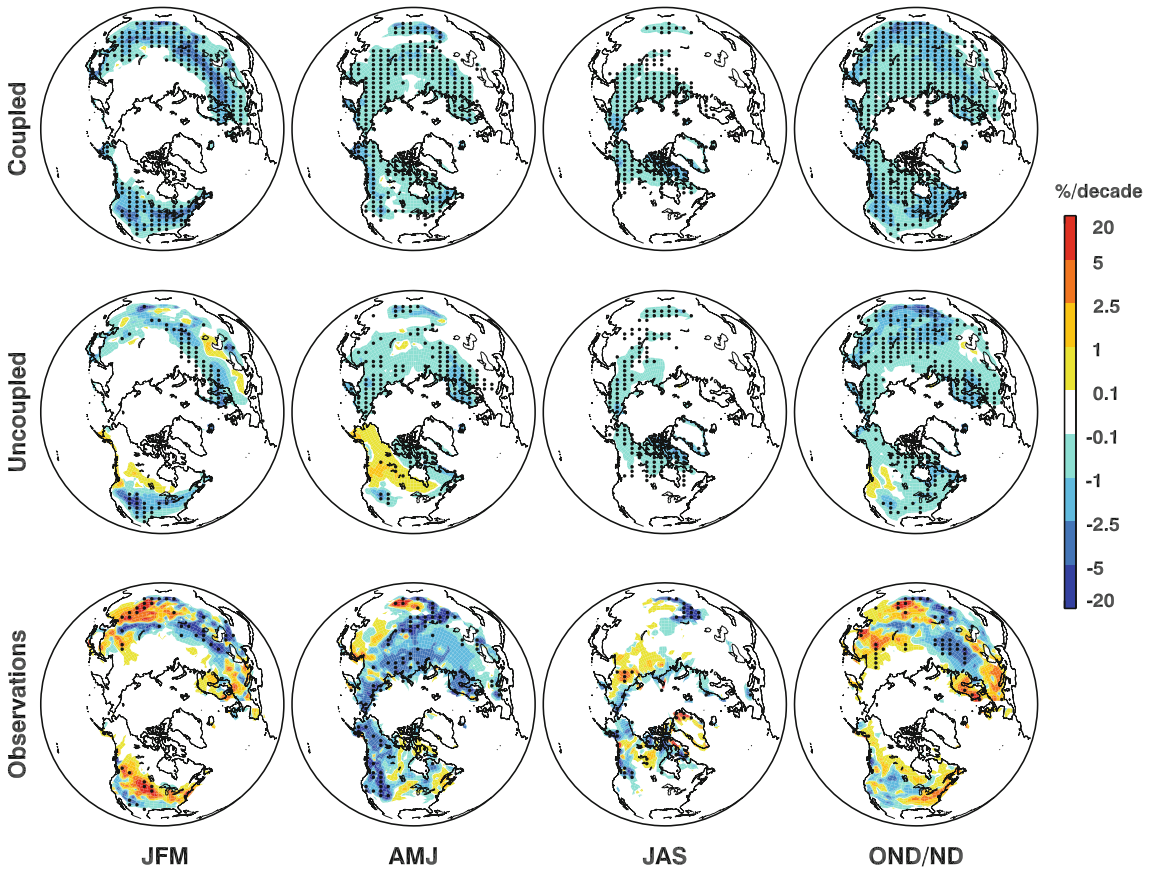

Fig. 6 (*Top*) Ensemble mean trend in snow cover fraction for the coupled experiment. (*Middle*) As top for uncoupled experiment. (*Bottom*) As top for NOAA snow chart CDR. *Stippling* indicates trend significance at the 95 % confidence level

wintertime reduction of SCE is strong in many of the realizations, which contrasts with the observations. This point is further quantified in Fig. 3, which shows the fraction of realizations with significant reduction trends in the coupled simulation as solid lines. It is seen that for every month at least 40 % of the ensemble produces SCE time series with significant trends for NH; this fraction is reduced for the individual continental regions, but the tendency towards snow reduction in all months and all regions is quite strong in the simulations. There are no months or regions with significant positive SCE trends in the coupled ensemble.

The tendency of the model to show too much loss of SCE in winter probably arises because the model is systematically biased towards excessive wintertime warming. Indirect evidence of this is shown in Fig. 4, which plots simulated and CRU observed land surface temperature trends in the same format as Fig. 2. For NH, NA, and EUR, the coupled ensemble shows systematically more warming than observed, and this warming is likely connected to the SCE reductions simulated in these periods. Additional indirect evidence is shown in the uncoupled simulation results in Figs. 2, 3, and 4. In these simulations, the wintertime warming is reduced, along with the number and fraction of realizations with significant SCE reductions. Generally speaking, the simulation of SCE trends in simulations driven by observed SSTs are closer to the observed record. We also note that NA trends are more sensitive to ocean SSTs than EUR trends; this difference reflects the relatively strong continentality of EUR climate (see discussion of Fig. 8).

The large ensemble dataset provides useful insight in this analysis. For example, while the SCE and temperature trends are systematically different between coupled and uncoupled experiments (Figs. 2, 4), the range of trends in the coupled and uncoupled simulations is for the most part similar (as seen by comparing interquartile ranges and the extent of the vertical lines). This result implies that natural variability in the coupled land-atmosphere system can drive much of the variability in the SCE and temperature trends, even in the absence of additional coupling to the oceans. The ensembles also reveal regions and seasons where clear discrepancies between the simulations and the observations are seen. We have discussed the case of wintertime warming and snow loss. There are also the significant positive trends in observed SCE seen during October for NH and EUR; corresponding significant positive trends in SCE are not found in any of the `coupled` or

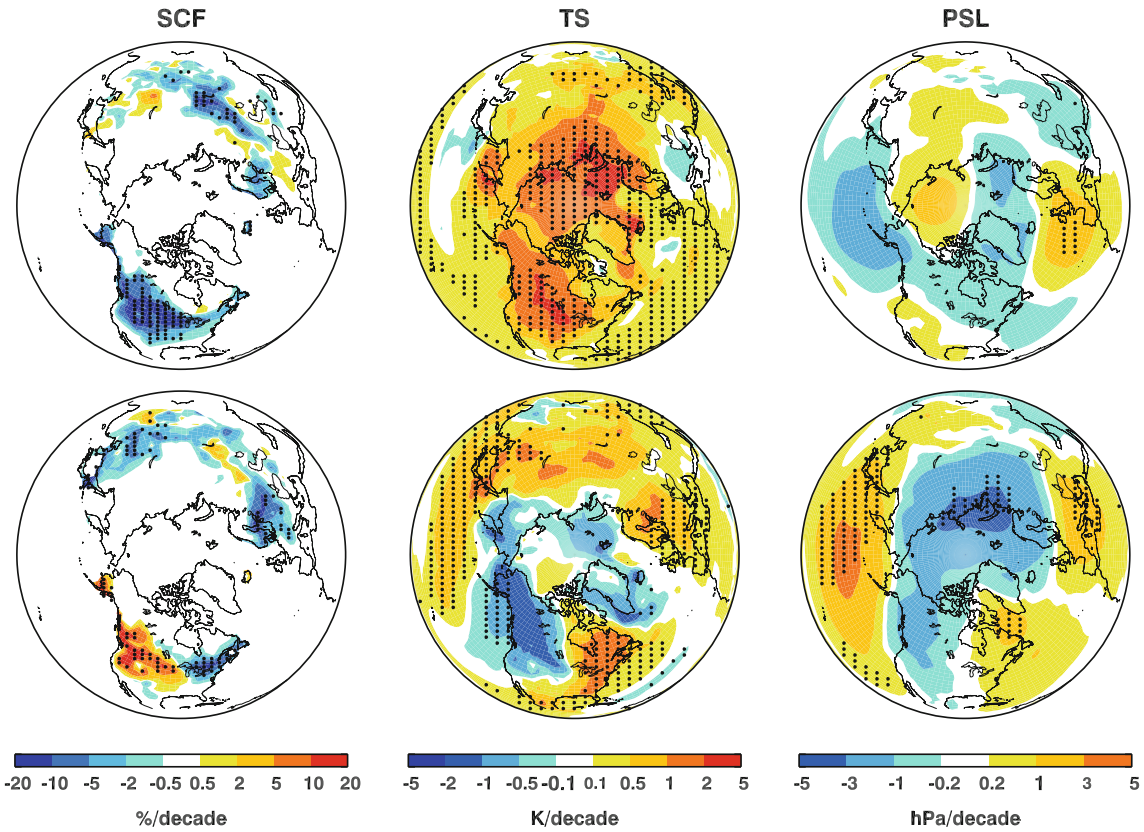

Fig. 7 JFM trends in snow cover fraction (*left*), surface temperature (*middle*) and sea-level pressure (*right*) for two selected coupled realizations. *Stippling* indicates trend significance at the 95 % confidence level

uncoupled realizations (Fig. 2, shaded bars). These trends are consistent with analysis of this data product by Cohen et al. (2012) and Liu et al. (2012); however, they are challenging to reconcile with fall season surface temperature warming trends across the region (Fig. 4 and numerous other studies). Brown and Derksen (2013) have examined the October Eurasian trend in the NOAA SCE CDR and have determined that it is primarily driven by an internal bias in the amount of snow cover charted over the 1982–2005 period. They further show that the trend is inconsistent with trends in other independent data sources including surface observations, reanalyses, and satellite passive microwave retrievals. The authors suggest that an increasing ability to detect small amounts of snow (due to increasing observational frequency and resolution) may be responsible for the trend seen in the NOAA CDR. Such an effect would be especially prominent during the shoulder seasons and lead to an increased potential to detect snow onset during the fall and an increased potential to detect snow disappearance in the spring.

Figure 5 summarizes how Brown and Derksen's analysis affects the agreement with the October SCE trends in the simulations. Examining trends in the original NOAA CDR over the three different regions described in the figure caption indicates that the trend in a geographically reduced analysis region where independent Eurasian ground observations are available is representative of the trend in the entire Eurasian region, which itself dominates the NH trend. This inference suggests that a large bias in the Eurasian trend would also prominently bias the NH trends. Adjusting the NOAA product time series so that its trend is consistent with ground observations leads to a reversal in both the trend sign and significance and brings the magnitude into agreement with both model results.

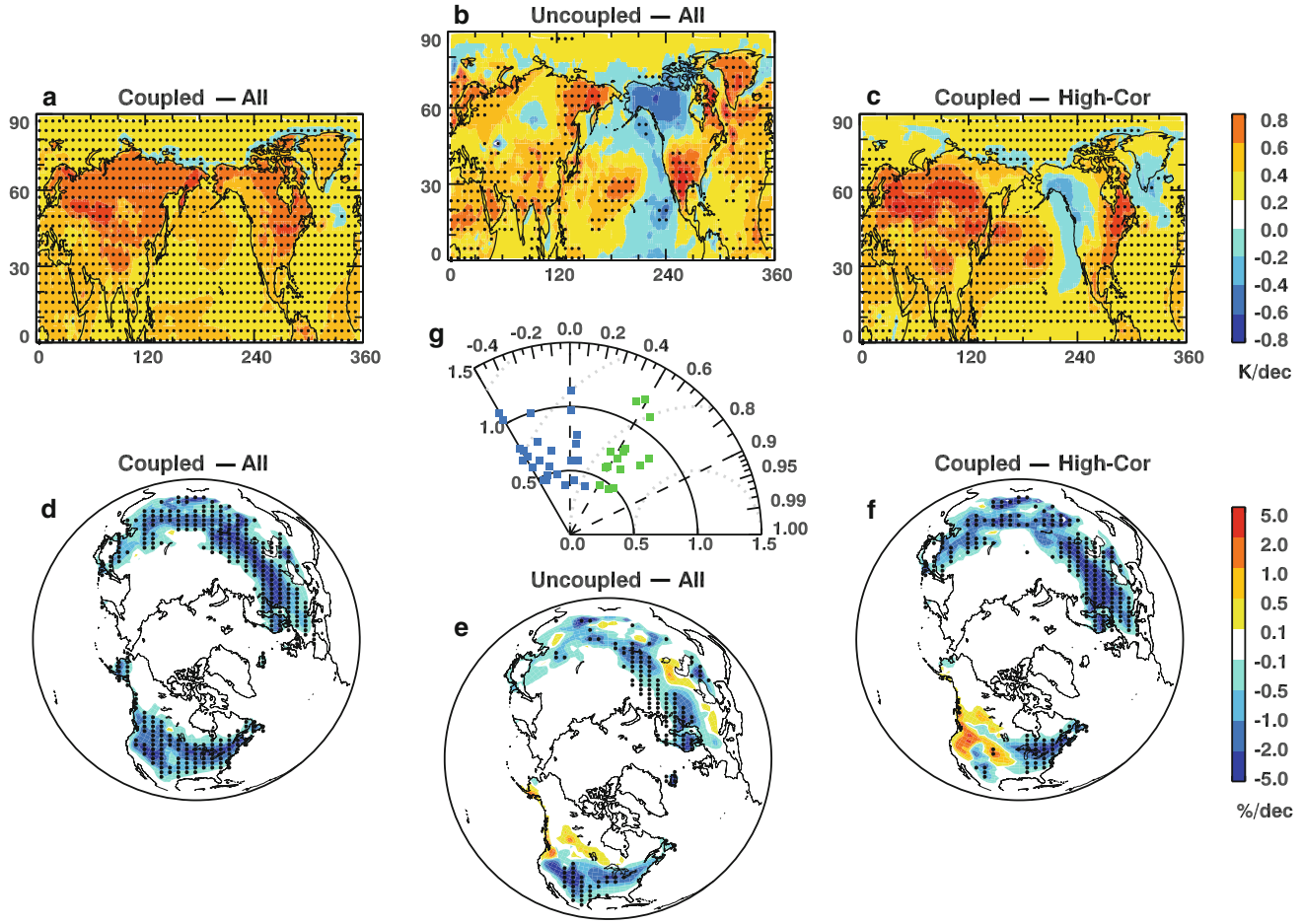

Fig. 8 JFM trends in SSTs superimposed with land surface temperature trends for **a** coupled ensemble, **b** uncoupled ensemble, **c** and 15 member subset of the coupled ensemble defined using panel (**g**). **d–f** as in (**a**)–(**c**) but for SCF. The subset in (**c**) and (**f**) is selected with reference to panel (**g**). **g** Taylor diagram showing pattern correlation (azimuth) and root mean square difference (radius) of the SST trends in each coupled realization relative to the trend in the observed historical SSTs driving the uncoupled ensemble for the region 50E–275E, 0N–40N. The fifteen realizations used for (**c**) and (**f**) are represented by *green dots* and have SSTs that have pattern correlation with historical SST trends greater then 0.4. *Stippling* indicates trend significance at the 95 % confidence level

Finally, we note that during late springtime (May, June, July) the magnitude of the observed SCE trends over NH and EUR are also not captured by any of the simulations. Issues with model physics such as snow-melt sensitivity and albedo feedbacks may be contributing to the discrepancy.

Spatial maps of observed trends in snow cover fraction (SCF) show a great deal of spatial and seasonal variability (Fig. 6, bottom row). Widespread reduction in spring (AMJ) SCF is seen over both continents, but in winter (JFM) SCF decreases over western and northern EUR and southern NA, and increases over eastern EUR and northern NA. There are also mixed trends during the fall period (because of the bias in October snow cover, we only plot a November/December average for the observed SCF). In the ensemble mean of the simulations, there is a systematic tendency towards SCF loss in all seasons and regions, reflecting the broad continental trends shown in Fig. 2. This tendency towards hemispherically coherent and regionally consistent snow loss is somewhat reduced in the uncoupled simulations, particularly in AMJ, resulting from reduced warming and increased snow precipitation over northwestern NA (see discussion of Fig. 12).

The ensemble means of both the coupled and uncoupled simulations show less spatial structure than the observed trend pattern, as expected from the smoothing arising from averaging over a large number of realizations. Nonetheless the ensemble mean is not always representative of individual realizations, some of which show trend patterns of similar magnitude and spatial scale to the observed record. For example, JFM SCF trends from two coupled realizations that were selected because they have highly contrasting SCF trend patterns are shown in Fig. 7. The SCF trends in these two realizations are consistent with each realization's surface temperature and sea-level pressure trends. For example, a trend towards an intensified Aleutian low is coherent with a trend towards advective warming and SCF reduction over NA (Fig. 7, top row); the opposite holds for the other realization (Fig. 7, bottom row). Similar pairs of contrasting trend patterns can also be found in the uncoupled ensemble. Despite these contrasting patterns, the typical simulation shows more

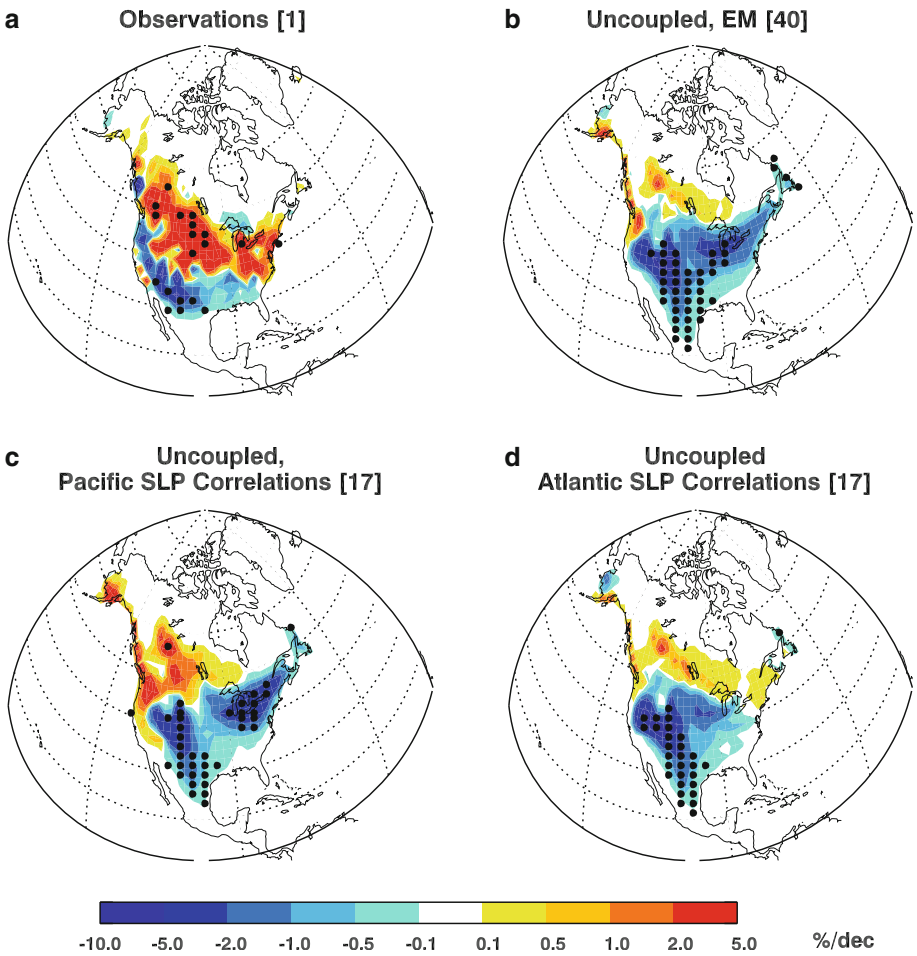

Fig. 9 JFM trends in SCF for **a** NOAA snow chart CDR, **b** uncoupled ensemble mean and **c**–**d** subsets of the uncoupled ensemble selected on the basis that the spatial pattern of a particular realization's SLP trend is correlated with the observed SLP trend with a coefficient greater than 0.4. The regions used for the correlation are the (**c**) North Pacific sector, 137E–237E, and the **d** North Atlantic sector, 75W–25E, both between 39N–77N. The number of realizations that contribute to each trend are displayed in brackets. *Stippling* indicates trend significance at the 95 % confidence level

warming and snow loss than observed, which is a qualitatively unrealistic feature.

Since excessive wintertime warming in the coupled experiment is reduced in the uncoupled experiment, it is worthwhile to examine which aspects of the SSTs explain regional differences. Fig. 8a–b shows that the coupled ensemble is characterized by excessive JFM North Pacific warming compared to the observed historical SST trends. We recall that these observed SST trends are present in the data set used to force the uncoupled experiment. In addition, the zonal gradient of warming in the Pacific is much weaker in the ensemble mean of the coupled realizations (Fig. 8a), and in the individual coupled realizations (not shown), than in the observations as represented by the uncoupled experiment SSTs (Fig. 8b). Associated with the coupled ensemble's strong ocean warming and weak North Pacific dipole is a relatively uniform and large magnitude warming over NA (see Shin and Sardeshmukh 2011). The pattern of snow loss in these two ensembles (Fig. 8d–e) reflects this difference in temperature trends.

Because natural climate variability gives rise to a range of spatial patterns of the trends in the coupled simulations, it is instructive to pick a subset of coupled simulations whose SST trends most closely resemble the observed SSTs that are driving the uncoupled simulations. This selection is carried out with reference to the Taylor diagram (Taylor 2001) shown in Fig. 8g (see caption for details). The Taylor diagram shows that 1) spatial gradients in individual realization SST trends are weaker than observed and 2) individual coupled realizations are generally weakly spatially correlated with the observations. But there are a set of fifteen realizations (green points) whose spatial correlation with the observed SST trends is generally stronger. The composite mean surface temperature (Fig. 8c) and SCF (Fig. 8f) of this fifteen-member subset show reduced warming and/or cooling over northwestern NA, with a coincident pattern of increasing SCF; trends in Eurasia are relatively unaffected. A second composite of coupled realizations that shows strong anti-correlations with the historical SST trends (not shown) produces an oppositely signed dipole pattern in the North Pacific (as expected) associated with increased warming in northwestern NA and strong, negative trends in SCF in the same region. Results (not shown) are similar for the spring (AMJ) season and for the annual average.

Overall, the relatively weak direct correspondence between observed NA SCE trends and those in the coupled model appears strongly influenced by the simulated North Pacific temperature trends. However, we note that the tropical Pacific represents another possible source of the discrepancy. The tropical Pacific temperature trends seen in Fig. 8a not only have more warming than the historical trends in Fig. 8b, but also a different pattern. The pattern of tropical Pacific warming has been shown to influence land surface temperature and precipitation patterns as identified by Shin and Sardeshmukh (2011).

In addition to SST variability, Fig. 7 suggests that decadal variability in sea level pressure (SLP) may also play an important role, driving trends in surface temperature and subsequently snow cover. In Fig. 9 we perform a similar analysis to that shown in Fig. 8, selecting realizations on the basis of their pattern correlation with observed SLP (from the NCEP reanalysis product, Kalnay et al. 1996). As for SSTs, the greatest SCE trend sensitivity is seen over NA so we focus on that region. We perform this analysis on the uncoupled ensemble. Selecting based on how well model SLP correlates with observed trends in the North Pacific (Fig. 9c) yields a pattern similar to the ensemble mean (Fig. 9b), but with enhanced snow cover increases in northwestern NA corresponding to enhanced cooling in the same region (not shown). By contrast, selecting realizations based on pattern correlation of North Atlantic SLP trends yields increasing SCE trends in northeastern NA. Both patterns share the roughly dipole structure of the observations: positive SCE trends at more northern latitudes and negative SCE trends at more southern latitudes. However, the region of NA with snow cover increases is

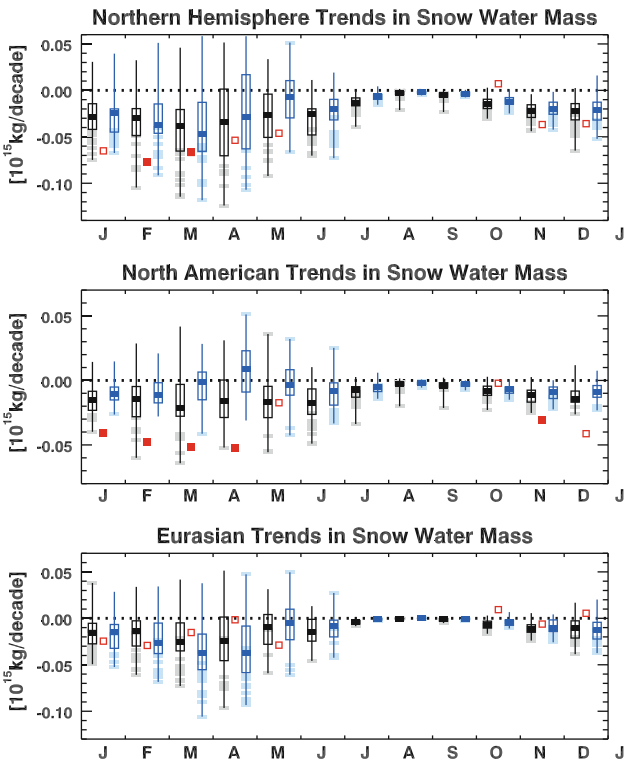

Fig. 10 As Figs. 2 and 4 but for SWM. Observational trends from the European Space Agency's GlobSnow product. Note that GlobSnow data are not available or of limited frequency and quality from June through September

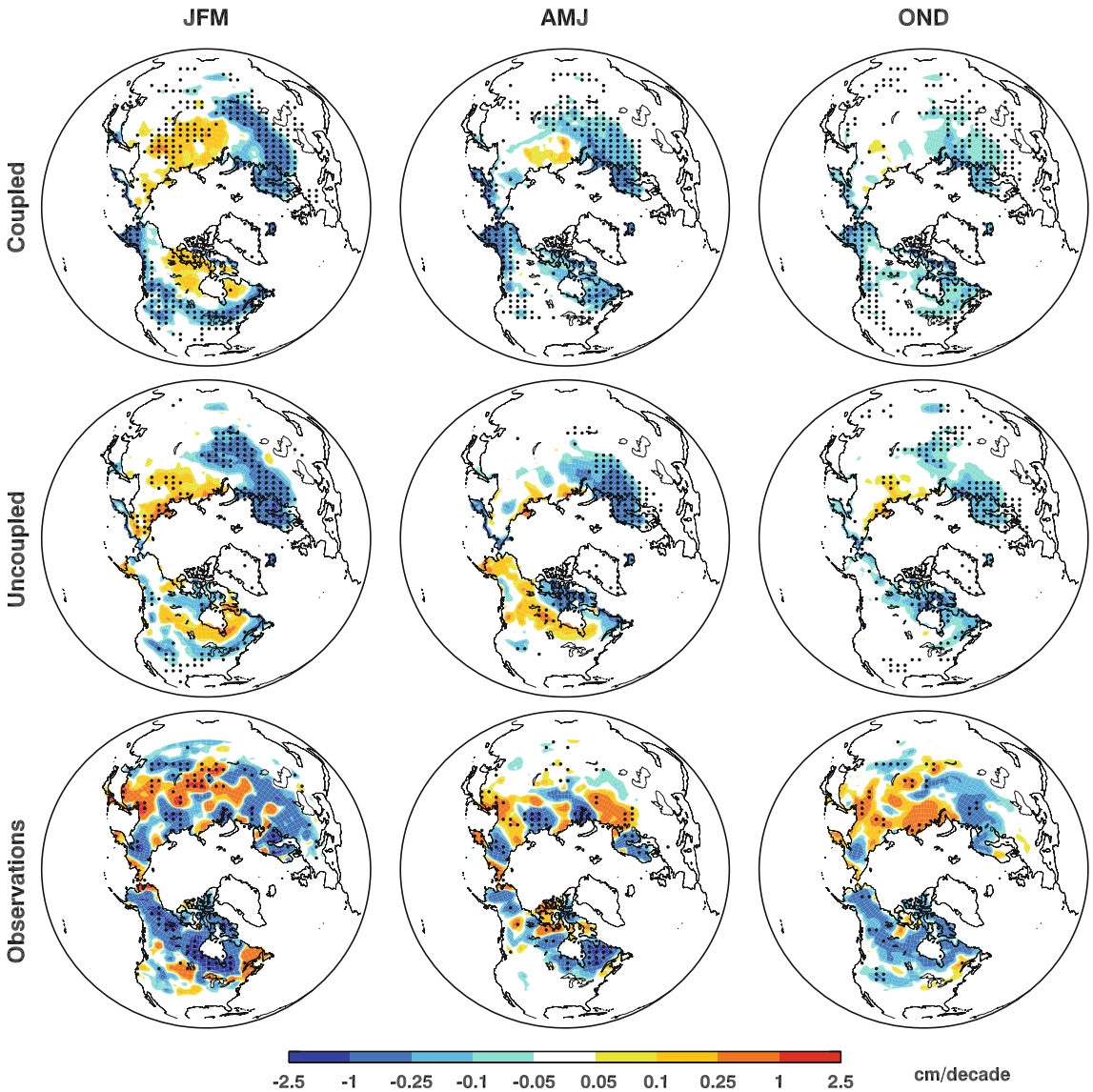

Fig. 11 (*Top*) Ensemble mean trends in SWE for the coupled experiment. (*Middle*) As top for the uncoupled experiment. (*Bottom*) As top for GlobSnow observations. *Stippling* indicates trend significance at the 95 % confidence level

located further north in the models than in the observations (Fig. 9a).

We note here that the observed SLP trends in the North Pacific and North Atlantic are not significant. Nonetheless the North Pacific trends tend to be reproduced in the `uncoupled` model and in the `coupled` realizations with SST trends similar to the observations and both circulation trends appear to consistently influence NA temperature and SCE trends.

3.3 Snow water equivalent trends

Unlike snow cover extent or fraction, snow water equivalent (SWE) or its spatial integral, snow water mass (SWM), represents a measure of accumulated snowfall and is thus controlled by temperature and precipitation trends. In general observed SWM trends (Fig. 10) are negative for NH and NA in winter (consistent with Takala et al. 2011) but are not significant for EUR. Model trends during JFMA show a qualitatively similar tendency towards SWM reduction over NA in the coupled simulations but not in the uncoupled simulations, reflecting strong thermal control by SSTs in that region for the simulations. In EUR, observed, coupled, and uncoupled wintertime trends are mixed. As a consequence of different trends in these regions, NH wintertime trends are also mixed.

We examine the spatial distribution of the SWE trends in Fig. 11. The Eurasian trends are very consistent between the coupled and uncoupled ensembles and show reasonable agreement with the GlobSnow trends over this region as well. In particular, all data sets indicate generally

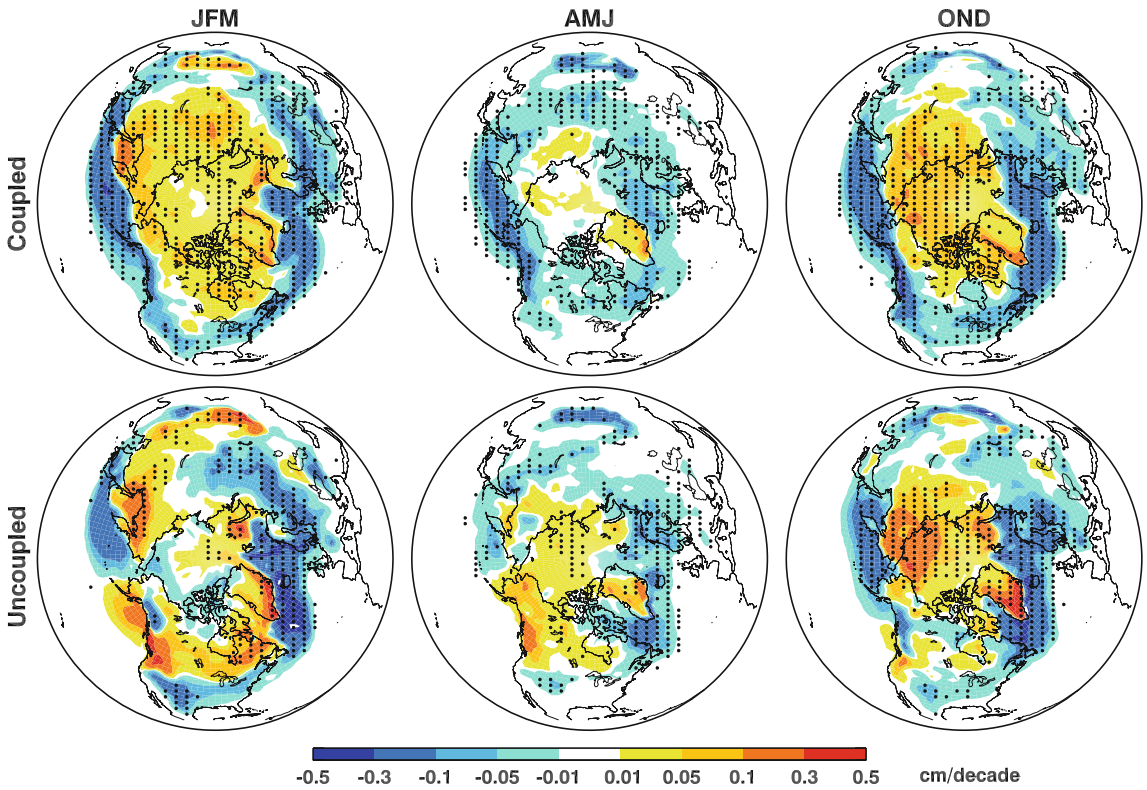

Fig. 12 (*Top*) Ensemble mean trends in average monthly precipitated snow-water for the coupled experiment. (*Bottom*) As top for the uncoupled experiment. *Stippling* indicates trend significance at the 95 % confidence level

decreasing trends over Europe and western Siberia and increasing or weak trends over eastern Siberia for all snow seasons. This result is consistent with the continental SWM trends presented in Fig. 10c. The spatial patterns are also consistent with results by Ghatak et al. (2012), linking the pattern of Eurasian SWE, surface temperature and snowfall trends to circulation changes initiated by September sea ice loss. The trends over NA differ more. The coupled model shows decreasing SWE over Alaska and northern Canada during spring and fall, in agreement with trends from the GlobSnow product. However, during winter there is increasing SWE over the Canadian archipelago and decreasing SWE across southern Canada and the northern US, in direct opposition to the strong significant decreasing trends seen in the GlobSnow product. The wintertime trends in the uncoupled ensemble mean are similar to the coupled experiment but show strong increases in SWE during the springtime. The discrepancy in location of the decreasing SWE suggests that the agreement between observed and simulated trends of total NA snow mass during JFMA may be for the wrong reasons. The region of decreasing SWE for both ensembles in Fig. 11 reflects the same region of decreasing SCF in Fig. 6 and occurs at latitudes far enough south that surface temperature changes may driving trends in both snow variables. By contrast, in the observations NA SWM and SCE evolve differently with significant wintertime reduction of SWM (Fig. 10) and weakly positive SCE trends (Fig. 2). Comparing their spatial patterns in Figs. 6 and 11, we can see that the region of SWE reduction occurs further north where the majority of the climatological snow mass exists, whereas the wintertime trends in SCE occur at lower latitudes of more limited snow depth.

The differences in North American SWE trends between the model experiment and the GlobSnow observations noted above are likely forced by snow precipitation trends present in the models; however, these precipitation trends may be themselves forced by temperature changes depending on their location. Examining the model snow water precipitation trends in Fig. 12 shows that they are highly correlated with the resulting SWE trends. In general these trends resemble those of liquid precipitation and consist of increased high latitude precipitation and decreased mid latitude precipitation. As expected, the resulting ensemble mean trend pattern in snow water precipitation has more zonal structure in the uncoupled experiment than in the coupled experiment. During AMJ (and JFM to a lesser extent) snow precipitation over northwestern NA has a strong influence on the `uncoupled` model trends in SWE (Fig. 11) as well as SCF (Fig. 6) in regions that would otherwise be susceptible to temperature-induced melting as seen in the `coupled`

experiment. For both seasons there is an associated cooling trend over the same region that both drives the increased snowfall and reduces snow melt. Likewise, during the winter we see that the pattern of low latitude drying and high latitude wetting is echoed in the simulated SWE trends of both experiments. However, over the Arctic ocean and surrounding land, the increase in snow precipitation is associated with warming trends and therefore is forcing changes in SWE via precipitaiton only. The change in snow precipitation change over the central Arctic is typical of future projections of climate models (Meehl et al. 2007). We reiterate here that the change in North American precipitation patterns seen in Fig. 12 for the `uncoupled` experiment is a result of the SST trends used to force the atmosphere. A similar composite of snow precipitation to that used in Fig. 8 shows that it is possible to obtain similar trend patterns of snow precipitation in the `coupled` experiment by selecting based on the SST trends.

4 Conclusion

We have analyzed Northern Hemisphere snow trends in the National Center for Atmospheric Research's Community Earth System Model with a focus on comparison to observations and an attempt to account for the impacts of natural variability using a large ensemble methodology. We generated two 40-member ensembles of the model driven by historical radiative forcings over the period 1981–2010, one coupled to a dynamical ocean (coupled) and the other driven by observed sea surface temperatures (uncoupled). Differences between these two ensembles demonstrate that the trends in seasonal snow cover parameters like snow cover extent/snow cover fraction (SCE/SCF) and snow water equivalent/snow water mass (SWE/SWM) over North America are strongly influenced by historical sea surface temperature trends in the North Pacific Ocean and by sea level pressure trends in the North Pacific/North Atlantic sectors. The former finding is consistent with previous results using realizations from multiple GCMs (Shin and Sardeshmukh 2011).

Climatology and variability of simulated SCE compare well with observations (Fig. 1). However, ensemble mean trends in snow cover extent from both experiments show unrealistically weak seasonality with overly strong negative SCE trends during winter and overly weak trends during the spring (Fig. 2). While we cannot rule out natural variability affecting the magnitudes of snow reduction in the observations, the snow reduction biases reported in the coupled model are consistent with overly strong and seasonally consistent warming trends (Fig. 4). Additional evidence is seen in the uncoupled simulations which have less wintertime warming and a corresponding reduction in both magnitude and significance of winter season SCE loss (Figs. 2–4).

The model climatology and variability for SWE are reasonable across the non-alpine regions available for comparison with the GlobSnow data record, but do illustrate a positive bias during spring (Fig. 1). Both model configurations agree on the magnitude of Eurasian trends throughout the year and the magnitude and seasonal cycle are broadly consistent with the observed values; however, North American trends differ in both respects between each model configuration and the observations (Fig. 10). Examining the spatial distribution of trends reinforces these conclusions: both models show a pronounced east-west dipole over Europe and Siberia consistent with observations but fail to agree over North America (Fig. 11).

For both SCE and SWE the differences between the coupled and uncoupled ensemble mean trends are connected to differing mean temperature and precipitation trends. Within each ensemble natural climate variability generates widely different spatial patterns of snow trends, but the SCE and SWE patterns in each realization can be related in an intuitive way to the corresponding temperature, precipitation and circulation trends of the given realization (Figs. 7 and 11–12). These land surface temperature and precipitation trends are in turn related to the patterns of SST trends (Fig. 8) and SLP trends (Fig. 9) in the model. Thus, while the coupled model ensemble mean SST trends lead to a strong snow reduction signal over North America on average, a subset of realizations from that experiment that show better correlation with the historical SSTs and also show similar trends in SCF and SWE as the uncoupled ensemble mean. In the uncoupled model, whose SST trends correlate perfectly with the historical trends, it is possible to discern how intra-ensemble variability in regional SLP trends alters the patterns of SCE trends, especially over North America. The influences of these trends appear to be consistent despite the fact that they are relatively weak with respect to their variability.

These climate system connections demonstrated within model realizations also aid the interpretation of the observational record. The strong influence of North Pacific SSTs on the model's snow trends suggests that the pattern of observed SST trends over the last three decades may have also influenced observed snow trends. A simple extrapolation of the same effect seen within the model would indicate that the amount of snow loss observed over northwestern NA for the past thirty years could have been intensified in a world with differing SST trends. On centennial time scales the signal of anthropogenically forced climate change will eventually overwhelm even regional scale natural variability, including that linked to decadal

time scale SST and SLP fluctuations. However, the strong influence of decadal trends in SSTs demonstrates the importance of properly simulating not only the magnitudes but also the patterns of SST trends in climate projection experiments as well as decadal prediction experiments on time scales of up to 30 years.

Acknowledgments We acknowledge assistance through legacies of the fourth International Polar Year. We also acknowledge funding from the Natural Sciences and Engineering Research Council of Canada's Climate Change and Atmospheric Research initiative via the Canadian Sea Ice and Snow Evolution Network. In situ Russian observations provided coutesy of R. Brown and P. Groisman. Computations were performed at the SciNet HPC Consortium funded by: the Canada Foundation for Innovation under the auspices of Compute Canada; the Government of Ontario; Ontario Research Fund-Research Excellence; and the University of Toronto. We thank Clara Deser and an anonymous reviewer for comments which helped to greatly improve the manuscript.

References

Atkinson DE, Brown R, Alt B, Agnew T, Bourgeois J, Burgess M, Duguay G, Henry Gea (2006) Canadian cryospheric response to an anomalous warm summer: a synthesis of the climate change action fund project, "The state of the arctic cryosphere during the extreme warm summer of 1998". Atmos Ocean 44:347–375. doi:10.3137/ao.440403

Branstator G, Teng H (2010) Two limits of initial-value decadal predictability in a CGCM. J Clim 23:6292–6311. doi:10.1175/2010JCLI3678.1

Brown RD, Derksen C (2013) Is Eurasian October snow cover extent increasing? Environ Res Lett 8:024–006. doi:10.1088/1748-9326/8/2/024006

Brown RD, Goodison BE (1996) Interannual variability in reconstructed canadian snow cover, 1915–1992. J Clim 9:1299–1318. doi:10.1175/1520-0442(1996)009<1299:IVIRCS>2.0.CO;2.

Brown R, Derksen C, Wang L (2007) Assessment of spring snow cover duration variability over northern Canada from satellite datasets. Remote Sens Environ 111:367–381. doi:10.1016/j.rse.2006.09.035

Brown RD, Mote PW (2009) The response of northern hemisphere snow cover to a changing climate*. J Clim 22:2124. doi:10.1175/2008JCLI2665.1.

Brown R, Derksen C, Wang L (2010) A multi-data set analysis of variability and change in Arctic spring snow cover extent, 1967-2008. J Geophys Res 115:D16111. doi:10.1029/2010JD013975

Brown RD, Robinson DA (2011) Northern Hemisphere spring snow cover variability and change over 1922–2010 including an assessment of uncertainty. Cyrosph 5:219–229. doi:10.5194/tc-5-219-2011

Bulygina ON, Razuvaev VN, Korshunova NN (2009) Changes in snow cover over Northern Eurasia in the last few decades.Environ Res Lett 4:045026. doi:10.1088/1748-9326/4/4/045026

Bulygina ON, Groisman PY, Razuvaev VN, Radionov VF (2010) Snow cover basal ice layer changes over Northern Eurasia since 1966. Environ Res Lett 5:015 004. doi:10.1088/1748-9326/5/1/015004

Callaghan TV, Bergholm F, Christensen TR, Jonasson C,Kokfelt U, Johansson M (2010) A new climate era in the sub-arctic: accelerating climate changes and multiple impacts. Geophys Res Lett 37:L14705. doi:10.1029/2009GL042064

Cohen JL, Furtado JC, Barlow MA, Alexeev VA, Cherry JE (2012) Arctic warming, increasing snow cover and widespread boreal winter cooling. Environ Res Lett 7(1):014–007. doi:10.1088/1748-9326/7/1/014007

Derksen C, Brown R (2012a) Arctic terrestrial snow in "state of the climate in 2011". Bull Am Meteorol Soc 93:S148–S149

Derksen C, Brown R (2012b) Spring snow cover extent reductions in the 2008–2012 period exceeding climate model projections. Geophys Res Lett 39:L19504. doi:10.1029/2012GL053387

Derksen C, Brown R, MacKay M (2007) Mackenzie basin snow cover: Variability and trends from conventional data, satellite remote sensing, and Canadian regional climate model simulations. In: Woo M-K (ed) Cold region atmospheric and hydrologic studies: the Mackenzie GEWEX experience. Springer, Berlin pp 213–240

Déry SJ, Brown RD (2007) Recent Northern Hemisphere snow cover extent trends and implications for the snow-albedo feedback. Geophys Res Lett 34:L22504. doi:10.1029/2007GL031474

Deser C, Phillips A, Bourdette V, Teng H (2012) Uncertainty in climate change projections: the role of internal variability. Clim Dyn 38:527–546. doi:10.1007/s00382-010-0977-x

Frei A, Miller JA, Robinson DA (2003) Improved simulations of snow extent in the second phase of the Atmospheric Model Intercomparison Project (AMIP-2). J Geophys Res 108:4369. doi:10.1029/2002JD003030

Frei A, Robinson DA (1998) Evaluation of snow extent and its variability in the atmospheric model intercomparison project. J Geophys Res 103:8859–8872. doi:10.1029/98JD00109

Ghatak D, Deser C, Frei A, Gong G, Phillips A, Robinson DA, Stroeve J (2012) Simulated siberian snow cover response to observed arctic sea ice loss, 1979–2008. J Geophys Res 117(D23). doi:10.1029/2012JD018047

Gent PR, et al (2011) The community climate system model version 4. J Clim 24:4973–4991. doi:10.1175/2011JCLI4083.1

Groisman PY, Karl TR, Knight RW, Stenchikov GL (1994) Changes of snow cover, temperature, and radiative heat balance over the northern hemisphere. J Clim 7:1633–1656. doi:10.1175/1520-0442(1994)007<1633:COSCTA>2.0.CO;2

Gutzler DS, Rosen RD (1992) Interannual variability of wintertime snow cover across the northern hemisphere. J Clim 5:1441–1448. doi:10.1175/1520-0442(1992)005<1441:IVOWSC>2.0.CO;2

Hurrell JW, Hack JJ, Shea D, Caron JM, Rosinski J (2008) A new sea surface temperature and sea ice boundary dataset for the community atmosphere model. J Clim 21:5145. doi:10.1175/2008JCLI2292.1

Jones PD, Lister DH, Osborn TJ, Harpham C, Salmon M, Morice CP (2012) Hemispheric and large-scale land-surface air temperature variations: an extensive revision and an update to 2010. J Geophys Res 117:D05127. doi:10.1029/2011JD017139

Kalnay E, et al (1996) The NCEP/NCAR 40-year reanalysis project. Bull Am Meteorol Soc 77:437–472. doi:10.1175/1520-0477(1996)077<0437:TNYRP>2.0.CO;2

Lawrence DM, et al, (2011) Parameterization improvements and functional and structural advances in version 4 of the community land model. J Adv Model Earth Syst 3:45. doi:10.1029/2011MS000045

Liu J, Curry JA, Wang H, Song M, Horton RM (2012) Impact of declining Arctic sea ice on winter snowfall. Proc Natl Acad Sci 109(11):4074–4079. doi:10.1073/pnas.1114910109

Meehl GA, et al (2007) Chapter 10: global climate projections. In:. climate change 2007: the physical science basis. In: Solomon S et al (eds) Contribution of working group I to the fourth assessment report of the intergovernmental panel on climate change. Cambridge University Press, Cambridge

Min S, Zhang X, Zwiers F (2008) Human-induced arctic moistening. Science 320:518–520. doi:10.1126/science.1153468

Popova V (2004) Structure of multi-year variations of the snow cover depth in North Eurasia. Russ Meteorol Hydro 8:78–88. doi:10.1002/joc.1489

Popova V (2007) Winter snow depth variability over northern Eurasia in relation to recent atmospheric circulation changes. Int J Climatol 27:1721–1733. doi:10.1002/joc.1489

Räisänen J (2008) Warmer climate: less or more snow? Clim Dyn 30:307–319. doi:10.1007/s00382-007-0289-y.

Shin S-I, Sardeshmukh PD (2011) Critical influence of the pattern of tropical ocean warming on remote climate trends. Clim Dyn 36:1577–1591. doi:10.1007/s00382-009-0732-3

Takala M, Luojus K, Pulliainen J, Derksen C, Lemmetyinen L, Kärnä J-P, Koskinen J (2011) Estimating northern hemisphere snow water equivalent for climate research through assimilation of space-borne radiometer data and ground-based measurements. Remote Sens Environ 115:3517–3529. doi:10.1016/j.rse.2011.08.014

Taylor KE (2001) Summarizing multiple aspects of model performance in a single diagram. J Geophys Res 106:7183–7192. doi:10.1029/2000JD900719.

Taylor KE, Stouffer RJ, Meehl GA, (2012) An overview of CMIP5 and the experiment design. Bull Am Meteorol Soc 93:485–498. doi:10.1175/BAMS-D-11-00094.1.

Trenberth KE, et al (2007) observations: surface and atmospheric climate change. climate change 2007: the physical science basis. In: Solomon S, Qin D, Manning M, Chen Z, Marquis M, Averyt K, Tignor M, Miller H (eds) Contribution of working group i to the fourth assessment report of the intergovernmental panel on climate change. Cambridge University Press, New York, pp 235–336